Tectonophysics 582 (2013) 126–139

Contents lists available at SciVerse ScienceDirect

Tectonophysics

journal homepage: www.elsevier.com/locate/tecto

Crustal deformation of the Andean foreland at 31° 30′S (Argentina) constrained by magnetotelluric survey

Luz Amparo Orozco [a], Alicia Favetto [a,*], Cristina Pomposiello [a], Eduardo Rossello [b], John Booker [c]

[a] CONICET, INGEIS, Ciudad Universitaria, C1428EHA Buenos Aires, Argentina
[b] CONICET, FCEN - Dpto. Ciencias Geológicas, Universidad de Buenos Aires, C1428EHA - Buenos Aires, Argentina
[c] Department of Earth and Space Sciences, Box 351310, University of Washington, Seattle, WA 98195, USA

ARTICLE INFO

Article history:
Received 7 November 2011
Received in revised form 28 August 2012
Accepted 28 September 2012
Available online 5 October 2012

Keywords:
Magnetotellurics
Flat slab
Sierras Pampeanas
Terranes

ABSTRACT

Twenty-five new long-period magnetotelluric sites near 31.5°S were collected in a west–east profile. This profile and the previous one, aligned with and adjacent to the eastern end, have been merged to form a single profile of more than 700 km long, extending from the Precordillera to the Chaco-Pampean Plain.
The geotectonic scenario is characterized by a modern flat subduction zone of the Nazca plate located at a depth of around 120 km and clearly defined by the distribution of earthquake hypocenters recorded by local and regional networks. A "bulge" shape at 68.5°W, with an anomalous dip to the west, is observed within this segment. The smooth slab deformation might result from the restriction on eastward motion due to the presence of an electrically resistive zone. The magnetotelluric model shows that this thick zone of increased resistivity is found from shallow crustal levels to upper mantle depths. The bulge geometry allows hot fluids and volatiles to rise from the deeper asthenospheric wedge, and reach the lower crust reducing its viscosity and letting it flow. The zones of low resistivity in the lower crust show spatial correlation with the areas of foreland deformation from Precordillera to the Sierras Pampeanas and may also suggest a ductile regime.
Shear zones reactivated by Cenozoic faulting must necessarily have their roots in the levels of the ductile lower crust associated to conductive channels. The zone where the lower crust is closer to the surface coincides with the areas of greatest structural relief and erosion. The interface between the folded ductile lower crust and the brittle upper crust might act as the main level of décollement of the bordering structures between the Precordillera, Sierra de Pie de Palo and the Sierras Pampeanas. In addition, the geometry of the interface might be conditioning the vergence of those structures.

1. Introduction

The Andean orogeny in South America has undergone the Peruvian, Incaic and Quechuan deformation cycles – crustal shortening and thickening – since its origin about 100 Ma. Unusual crustal thickness in the Andes is mainly due to east–west shortening caused by rapid convergence at the Pacific margin where the Nazca and South American plates have been converging at varying rates since the Paleocene (Cobbold et al., 2007).

The geometry of the subducted slab shows continuous transitions from flat to steep along the Andean margin. Nevertheless, there is no agreement about the characteristics of these transitions. Some authors consider that the most probable mechanism is a tear in the slab (Barazangi and Isacks, 1976) while others support slab flexure or contortion (Bevis and Isacks, 1984; Hasegawa and Sacks, 1981). The average width and elevation of the Andes varies along the strike, as does the amount of shortening which correlates with changes in the dip of the subducting oceanic plates (Cobbold et al., 2007).

Beneath Chile and western Argentina, between 27°S and 33°30′S, the subducted slab descends to a depth of 120 km at a nearly 30° dip and becomes flat. It then expands to the east for several hundred kilometers before resuming its descent into the mantle. This subduction style seems to be related to the buoyancy effect generated by the anomalously thick oceanic crust (15–20 km). In this case the flat slab geometry correlates with the inland prolongation of the subducted Juan Fernández Ridge below the margin at 31°S (Alvarado et al., 2009; Gutscher et al., 2000).

In this region, the flat subduction has an important thermal impact resulting in a much cooler plate interface which might explain the apparent increase in coupling. This interplate coupling is greater above flat slab segments (released seismic energy is 3–5 times greater) than above steep slab segments (Gutscher et al., 2000). On the other hand, Jordan et al. (1983) and Smalley et al. (1993) suggest that increased interplate coupling above flat slab regions has been the reason for thick-skinned deformation in the upper plate, resulting in large-scale block type uplifts as in the Sierras Pampeanas (SP).

* Corresponding author. Tel.: +54 1147833022; fax: +54 1147833024.
E-mail address: favetto@ingeis.uba.ar (A. Favetto).

0040-1951/$ – see front matter © 2012 Elsevier B.V. All rights reserved.
http://dx.doi.org/10.1016/j.tecto.2012.09.030

Processes developed during flattening of the slab are determined by the eastward migration of magmatic activity (Kay et al., 1991), which enhances heat flux with the subsequent development of brittle–ductile transitions in the crust, favoring basement deformation. Dehydration of the slab during flat subduction hydrates and weakens the still relatively warm overlying continental lithosphere, giving place to a zone of compressive deformation (James and Sacks, 1999).

Thermal weakening of the crust produces a wave of shortening across the Andes and the consequent crustal thickening, which leads to phase transformation in the lower crust, from mafic granulite facies to eclogite (Kay et al., 1996; Meissner and Mooney, 1998). During the transition from flat slab to normal subduction, the eclogitization of crustal roots leads to delamination. Leech (2001) suggests that the presence of fluids is the key in the process of eclogitization and delamination. On the other hand, Meissner and Mooney (1998) suggest that the onset of delamination results from the negative buoyancy (eclogite might provide such buoyancy) of the continental lower crust and sub-crustal lithosphere with respect to the warm, mobile asthenosphere. Another important aspect leading to delamination is the presence of a decoupling zone between the denser lithosphere and the lighter upper and middle crust. A delay of several million years may occur between the onset of delamination and the appearance of hot asthenospheric material at the crust–mantle boundary.

The magnetotelluric (MT) method is an important tool to study regional structures and may help to characterize processes in the crust and upper mantle. It has been successfully used to determine the presence of fluids, partial melt or other conductive anomalies. MT images the electrical resistivity, a parameter sensitive to temperature and to the presence of highly conductive fluids (water, melt), sulphides or graphite. The method has been applied in different environments and tectonic processes. An example is active continent–continent collision where MT allowed determining the content of fluid and the thermal structure which are key parameters for defining the rheology of the crust and upper mantle (Unsworth et al., 2005). In another study, zones of high electrical conductivity identified in the forearc and backarc regions were interpreted to be a consequence of fluid release from subducting slab (Soyer and Unsworth, 2006). Other applications were a study of the fluid distribution in a fault zone (Bedrosian et al., 2004) and the determination of the crust–mantle boundary over cratonic regions (Shalivahan and Bhattacharya, 2002).

We present a regional study of the effects of changes in slab geometry over the lithospheric structure in the Andean foreland. The analysis of these results takes into consideration previous geological and geophysical studies, mainly, of seismic hypocenter data recorded by local and regional networks (CHARGE, Chile–Argentina Geophysical Experiment and NEIC, National Earthquake Information Center) between 29°–33°S and 73°–63°W.

2. Regional setting

The older rocks in the west of South America are made up of pre-Carboniferous terranes amalgamated in the western border of Gondwana continent. The location of crustal block boundaries and their geometry at depth is in some cases controversial because the boundary is often defined on the basis of relatively limited surface and borehole geologic information and seismic reflection data. However, marked differences in composition are observed in exposed pre-Andean basement rocks in the accreted terranes.

The south central Andes region between 27° and 33° 30′S is tied to the flat subduction of the Nazca plate beneath South America at about ~120 km deep before descending into the mantle. The convergence rate is about 6.7 cm/yr in the N78°E direction (Vigny et al., 2009). Although there is no consensus about the drivers of flat subduction, Gutscher et al. (2000) suggested that it was caused primarily by the overthickened oceanic crust (15–20 km) due to the presence of the Juan Fernández Ridge. The collision effect propagated from North to South from ca. 18 to ca. 11 Ma, resulting in a southward diachronic beginning of basement block uplift. The main characteristic in the flat slab segment is the propagation of arc magmatism toward the foreland that generates thermal weakening of the crust and development of brittle–ductile transitions that allowed the uplift of the SP basement (Ramos et al., 2002).

In the Andean foreland, orogenic deformation uplifted the Precordillera (PC) and the SP from West to East (Fig. 1) by reactivating steep faults which become subhorizontal in depth (González Bonorino, 1950; Introcaso et al., 1987).

The PC forms the foothills of the Andes between 29° and 33°S. It is a fold and thrust belt laid over Paleozoic sedimentary rocks as a result of migration to the eastern orogenic front. It consists of three longitudinal belts. The Eastern belt has high angle faults with west vergence. These structures do not expose the basement, and they exhibit a thick-skinned deformation similar to the structure of the SP (Ortiz and Zambrano, 1981). The Western and Central PC can be considered together as a thin-skinned fold-thrust belt. The basement of the PC is only known through xenoliths of Miocene volcanic rocks, which are interpreted as rocks from the Cuyania basement of Grenville ages (ca. 1.1 Ga; Kay et al., 1996). The PC and the Sierra Pie de Palo (Western SP) have been interpreted as Cuyania composite block (Ramos, 1994).

The SP are basement blocks uplifted and tilted by steep faults with East and West vergence. They are composed of Neoproterozoic and Lower Paleozoic metamorphic and igneous rocks. Based on the magmatic and tectonic lithological associations, they were divided into two broad regions according to Caminos (1979): Western SP and Eastern SP. The Western SP are characterized by abundant basic and ultrabasic rocks, micacite, gneiss, crystalline calcites, amphibolites and scarce granitic bodies. The Eastern SP are composed of schists, gneisses and granitic rocks that reach batholitic dimensions, and abundant migmatites and granulites (Kraemer et al., 1995; Varela et al., 2000 among others). Regional metamorphism is attributed to the Pampean (Early Cambrian ~530 Ma) and Famatinian (Ordovician ~490 Ma) orogenies (Pankhurst and Rapela, 1998; Rapela et al., 1998; Thomas and Astini, 2003 and references therein). Older crustal discontinuities in the foreland, i.e. sutures and shear zones played a major role in the inception and geometry of the main faults that differentially uplifted the blocks of the SP (Ramos, 1994). Furthermore, seismic activity of the continental crust is very intense above the flat slab segment (Gutscher et al., 2000). Western SP are characterized by higher P-wave seismic velocities (6.2–6.4 km s^{-1}), lower S-wave seismic velocities ($Vp/Vs = 1.80–1.85$) and a thicker crust (45–52 km). Characteristics of Eastern SP are Vp of 6.0–6.2 km s^{-1}, Vp/Vs ratio of 1.65–1.70, and a thickness of 27–37 km (Alvarado et al., 2005).

One of the most important structures across the MT profile is the Valle Fértil Lineament, located in the western part of the Sierra de Valle Fértil with NNW–SSE direction and 600 km in length (Fig. 1). It is a first order morphostructure that controls the architecture of both the Precambrian–early Paleozoic crystalline basement and its sedimentary cover.

There are different hypotheses about the geotectonic development of the Valle Fértil Lineament: a) major crustal discontinuity cutting most of the crust and coinciding with an Early Paleozoic suture between the Cuyania and Pampia (or Pampean) Terranes (Ramos et al., 1993; Rapela et al., 2001; Zapata and Allmendinger, 1996), b) parautochthonous Cuyania Terrane located into the present position from Devonian times following mechanical wrenching (Aceñolaza et al., 2002; Finney, 2007), and c) intracontinental structure with recurrent tectonic activity. Different alkaline volcanic intrusions with Ar/Ar relationships indicate a deep intracontinental origin. This supports the idea of a persisting crustal discontinuity along this lineament, which evidences important Paleozoic, Mesozoic and Cenozoic deformations (Rossello et al., 2005).

The oblique Andean convergence caused the Valle Fértil Lineament to exhibit a thick-skinned tectonic style, which includes left-lateral transpression, marked by high angle reverse faults, *en echelon* folding of the sedimentary cover and intrusion of associated basaltic dykes.

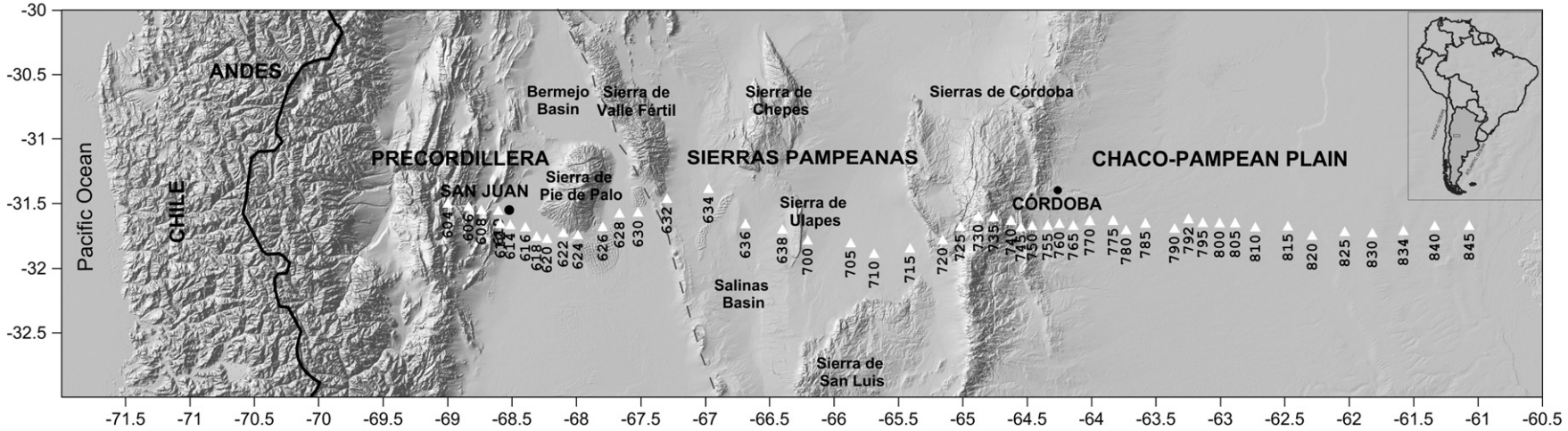

Fig. 1. Location of the study area and MT-sites profile (from Precordillera to the Chaco-Pampean Plain, across the Sierras Pampeanas). Main morpho-structures associated with Cenozoic tectonics in northwestern Argentina and the intermontane basins.

Rossello et al. (2005) have interpreted a positive flower structure with asymmetrical development and marked westward vergence from deep seismic, surface geology and structural data.

The Río de La Plata craton (RPC) consists of a Paleoproterozoic nucleus with little influence of Neoproterozoic orogenic events (Basei et al., 2000; Cingolani and Dalla Salda, 2000; Dalla Salda, 1999; Hartmann et al., 2003; Pankhurst et al., 2003; Saalmann et al., 2005 and references therein). Towards the west, the RPC is covered by the very thick Phanerozoic sedimentary deposits of the Chaco-Paranaense basin. The juvenile Paleoproterozoic ages and isotopic signature in the outcrops of the RPC in Argentina correspond to localities in Tandilia and to boreholes in the west of the Chaco-Paranaense basin (Pankhurst et al., 2003; Rapela et al., 2005) (see Fig. 1).

3. Electrical resistivity

Electrical conduction in Earth materials is mainly due to the flow of ions in fluids or electrons in solids. So, high conductivity values indicate the presence of interconnected fluids or minerals and generally dry rocks are highly resistive. MT models show the distribution of electrical resistivity which is very sensitive to the temperature and to the presence of highly conductive fluids (water, melt, graphite, etc.). In regions of active deformation, these are mainly partial melts and saline fluids whose resistivity is much lower than that of the rock matrix. Circulating currents are determined by the amount of fluid distributed within the rock.

High conductivities associated with lower crust have been interpreted by the existence of interconnected minerals such as graphite, oxides and sulphides, and saline pore fluids. Values in the lower crust of young tectonic areas range from 10 to 30 Ωm, increasing to 100–300 Ωm in the older areas (e.g. Hyndman and Shearer, 1989; Shankland and Ander, 1983).

Graphite might be present in different environments, such as stable regions, active orogens, exhumed shear zones in orogenic belts, and also may be able to explain the high conductivity in ancient collision zones (Glover and Ádám, 2008; Losito et al., 2001).

Crustal and upper mantle rocks and fluids can be related to partial melt. Rock strength decreases with increasing melt fraction. The most significant variation in strength is observed when the melt fraction varies by 10% (Rosenberg and Handy, 2005).

4. Crustal thickness of the southern central Andes

The depth to the Moho discontinuity has been inferred by many authors, mainly based on seismological studies, which determined a greatly increased compressional seismic velocity. The presence of a clear Moho arrival is indicative of a significant velocity contrast between the crust and mantle. This compositional discontinuity is commonly assumed to separate mafic lower-crustal rocks from upper mantle ultramafic rocks.

Lateral variations in the crustal thickness through Chilenia, Cuyania and Pampia Terranes were shown in previous geophysical studies of the Gilbert et al. (2006) identified variations in crustal thickness and in the signature of the Moho along this zone from a P wave receiver functions study obtained from a teleseismic recordings belonging to a local seismologic network the Chile Argentina Geophysical Experiment (CHARGE, Wagner et al., 2005). They observed and interpreted the lack of a strong Moho signal in the Western SP as a small impedance contrast caused by eclogitization of a thickened lower crust. The thick crust was found to be over 60 km beneath the Andes and to extend ~200 km to the east up to the Western SP, where thickness starts decreasing eastward. In addition, Heit et al. (2008) used CHARGE array and successfully detected S to P converted waves from the Moho through S wave receiver functions. The crust reaches its maximum thickness of ~70 km (along 30°S between 70°W and 68.5°W) beneath the Principal Cordillera and the Famatina system and becomes thinner towards the SP with a thickness of about 40 km. Recently, Gans et al. (2011) used P wave receiver functions to image the subsurface of the Pampean flat slab region using the dense SIEMBRA array (The Sierras Pampeanas Experiment using Multicomponents Broad band Array) combined with the broader CHARGE and ESP arrays and the depth estimate to the continental Moho map could be improved. In Table 1, a list of values inferred by different authors is shown.

5. MT method

Magnetotellurics (MT) is a natural-source electromagnetic (EM) geophysical method. EM fields with periods shorter than 1 s are mainly originated by worldwide lightning discharges. The interaction between the Earth's magnetosphere (and ionosphere) and solar wind generates fluctuations with periods longer than 1 s. These natural external variations used in MT studies induce electric currents in the Earth and have periods between 10^{-3} and 10^{5} s. The EM skin depth that depends on the electrical resistivity of the Earth and the period of the signal restricts maximum penetration.

Measurements of time-varying EM field components at the Earth's surface allow calculating the transfer function which is complex and frequency (f) dependent. The relationship between horizontal electric and magnetic components at different frequencies is used to define the MT impedance tensor, $Z(f)$. The vertical and horizontal magnetic components are described by the transfer function, $T(f)$. The elements of MT Z (2×2 tensor) are transformed into apparent resistivity, $\rho(f)$, and phase, $\varphi(f)$, and the real and imaginary parts of the transfer function represented as induction arrows which point to conductive zones (Parkinson, 1962).

For a 1D layered Earth, Z is diagonal and T elements are exactly zero and the off-diagonal elements of Z are equal in magnitude and opposite in sign. In 2D structures, resistivity is constant in strike direction and varies with both the perpendicular to strike direction and depth. In this case, data can be separated into two independent modes with electric current flowing parallel (TE) and perpendicular (TM) to the strike direction.

Table 1
Crust thickness (km) in the central Andes for Chilenia, Cuyania and Pampia Terranes determined by different methods at 31°S.
Modified from Alvarado et al. (2010) and new data (Gans et al., 2011).

Chilenia Terrane	Cuyania Terrane	Pampia Terrane	Method	Reference
	52–60		S-to-P converted seismic phases on the Moho	Regnier et al. (1994)
65	55	35	Seismic moment tensor inversion	Alvarado et al. (2005)
70	60	30	Gravimetry	Introcaso et al. (1992)
64	50	40	Teleseismic P-wave receiver functions	Gilbert et al. (2006)
	52		P-wave receiver functions obtained using intermediate-depth local events	Calkins et al. (2006)
60	55		Direct modeling of broadband seismic waves	Alvarado et al. (2007)
60	50	36	P_n-wave refraction	Fromm et al. (2004)
75	58		From teleseismically recorded depth phase precursors	McGlashan et al. (2008)
	70	50	Teleseismic S-wave receiver functions	Heit et al. (2008)
64	54	49	Receiver function analysis (maximum depth to Moho near 31°S)	Gans et al. (2011)

5.1. Data acquisition and processing

Surface field measurements were made of the orthogonal electric (*Ex*, *Ey*) and magnetic (*Hx*, *Hy*, *Hz*) field components, with axis directions defined as follows: *x* to the North, *y* to the East and *z* toward the subsoil. The electric field was measured with pairs of Pb–$PbCl_2$ electrodes at a distance of around 100 m. The magnetic field was measured with "flux gate" type magnetometers recorded in the range of 1 to 10,000 s.

The profile is located at around 31.5°S and has west–east direction; the new sites have been added at the western end of the previous profiles (Booker et al., 2004; Favetto et al., 2008). A total of 49 sites stretch along more than 700 km from the PC to the Chaco-Pampean Plain. Data were acquired between 2001 and 2006, using Long range Intelligent Magnetotelluric System (LIMS) for the MT sites 604 to 630 and Narod Intelligent Magnetotelluric System (NIMS) for MT sites 632 to 845.

Data were processed using robust multisite statistical time series methods (Egbert, 1997). Pseudo-sections of apparent resistivity (ρ) and phase (φ) for both polarizations as well as of the real and imaginary parts of the transfer function between the vertical and horizontal magnetic fields (*Tzy*) in measurement coordinates, for the period range of 10 – 10000 s are shown in Fig. 2a, b and c.

5.2. Dimensionality and distortion

The dimensionality and best geoelectrical strike estimation were obtained using phase tensor analysis (Bibby et al., 2005; Caldwell et al., 2004) and multisite, multifrequency tensor decomposition (McNeice and Jones, 2001).

Galvanic distortions, which are caused by the charge formed at the boundary of the near-surface conductivity heterogeneity, are commonly observed in MT surveys. They can be regarded as the superposition of the (frequency independent) signatures of (3D) heterogeneities on the (frequency dependent) signature of the larger-scale regional structure. In these cases, the horizontal components of magnetic fields are not

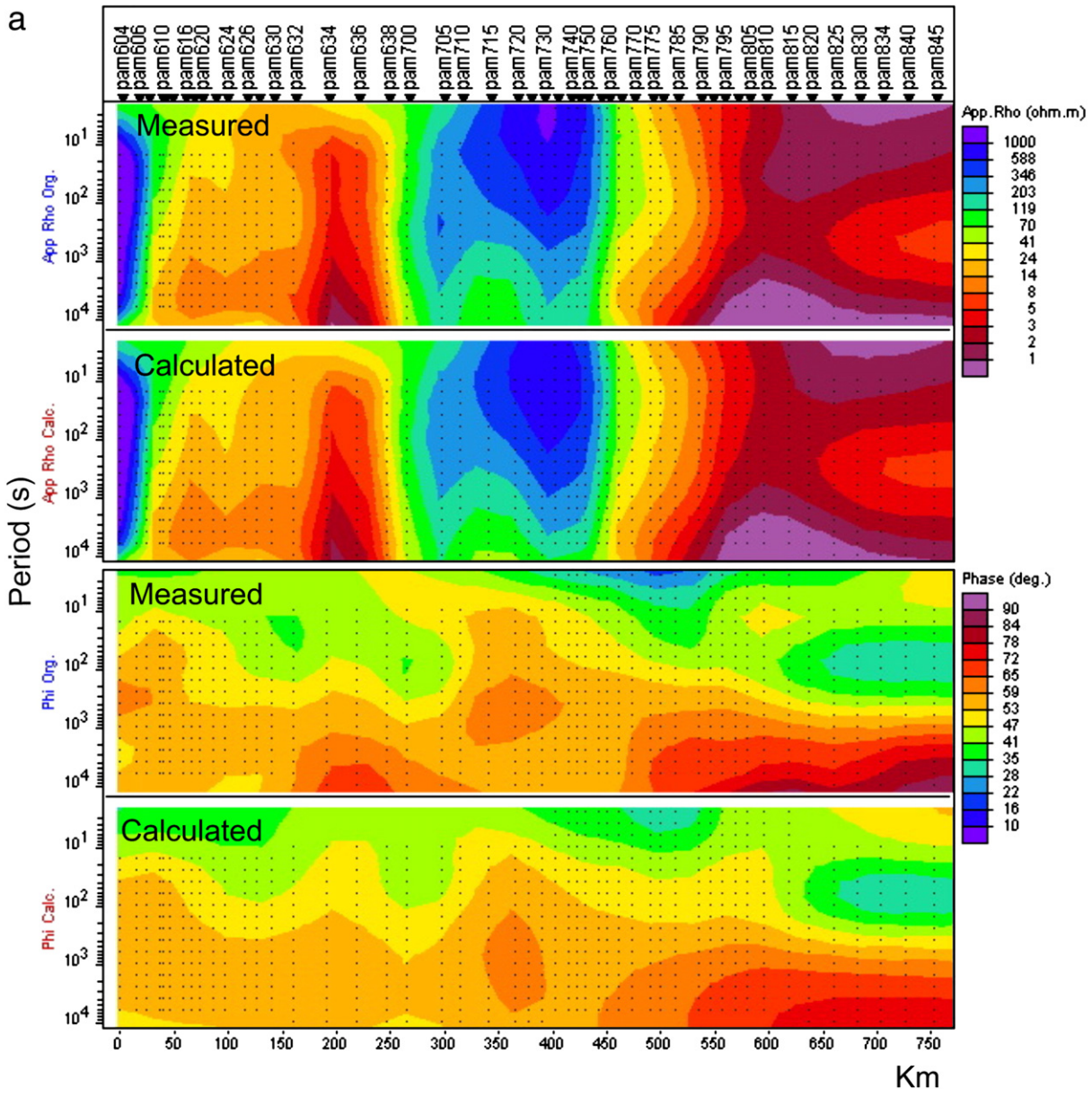

Fig. 2. a) MT data (Orig) and model response (Calc) pseudosections of apparent resistivity (App.Rho, Ωm) and phase (Phi, degrees) for TE polarization. b) MT data (Orig) and model response (Calc) pseudosections of apparent resistivity (App.Rho, Ωm) and phase (Phi, degrees) for TM polarization. c) MT data (Orig) and model response (Calc) pseudosections of real (Hz REAL) and imaginary (Hz IMG) parts of the transfer function between the vertical and horizontal magnetic fields, *Tzy*.

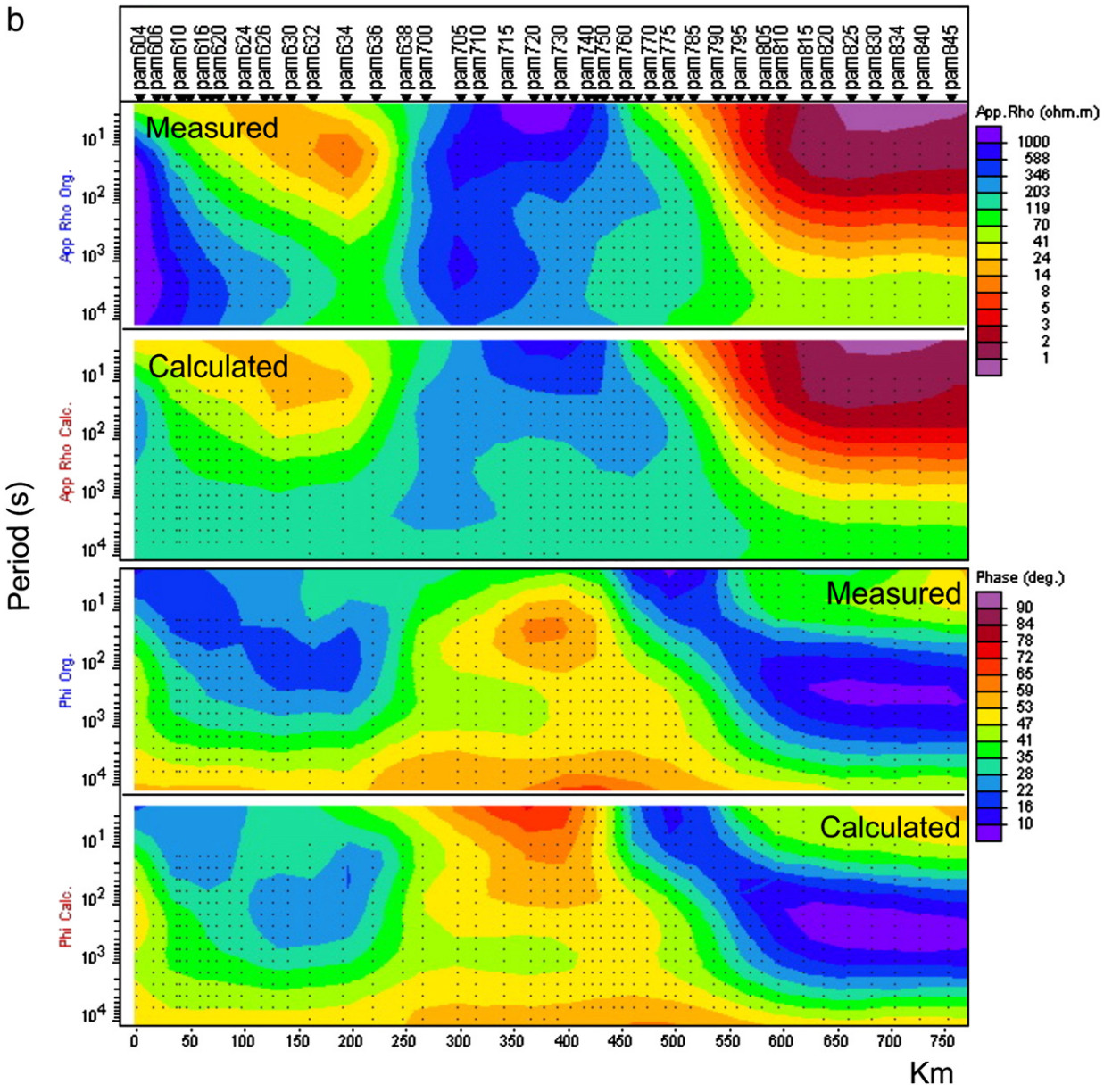

Fig. 2 (*continued*).

significantly affected and distortion is almost entirely confined to the electric field.

Consequently, when MT data contain galvanic effects, the observed electric field E can be expressed as

$$E(T) = E_R(f) + E_S(f) = DE_R(f)$$

where f is the signal frequency, E_R is the regional electric field (i.e. the field that would be observed at the surface in the absence of the heterogeneity) and E_S is the scattered or secondary electric field produced by the regional field on the local heterogeneity. D is the distortion tensor (2×2 real frequency-independent matrix).

The analysis of the phase tensor is a very useful tool to study the dimensionality of the structure. By splitting impedance tensors Z into real (X) and imaginary (Y) components $Z = X + iY$, a phase tensor Φ is defined as $\Phi = X^{-1}Y$.

The graphic representation of the phase tensor (and in fact of any 2×2 real matrix) is an ellipse. An invariant parameter of this tensor is the skew angle defined as:

$$\text{Skew angle} = 1/2\ \tan^{-1}((\Phi_{12}-\Phi_{21})/(\Phi_{11}+\Phi_{22})).$$

The phase tensor determines whether the 2D structure approximation is valid when its absolute value is less than 1.5° (Bibby et al., 2005). Another useful invariant, called ellipticity (λ) determines that the symmetry of the structure may be assumed to be 1D when it is smaller than 0.1. It is defined as:

$$\lambda = ((\Phi\max - \Phi\min)/(\Phi\max + \Phi\min)).$$

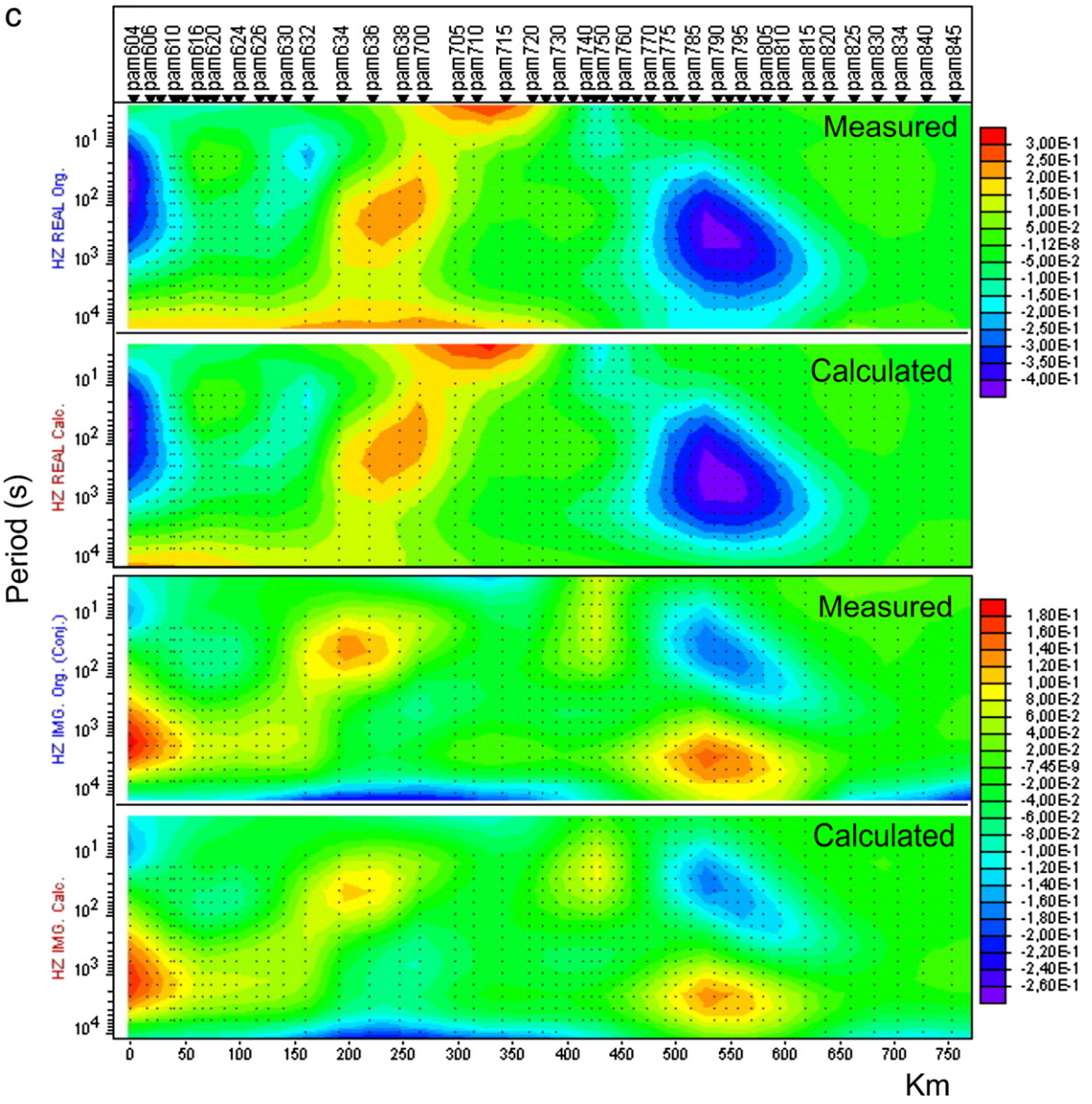

Fig. 2 (*continued*).

The galvanic distortion analysis developed by Groom and Bailey (1989, 1991) has become the most used method. This approach describes the observed impedance tensor Z as

$$Z = \mathrm{R}CZ_{2D}\mathrm{R}^{T}.$$

R is a rotation matrix, which rotates vectors by an angle θ (regional 2D strike) from the regional measurement axis system to the measurement axis system, C is a real 2×2 telluric distortion tensor, and Z_{2D} is the 2D regional impedance tensor in strike coordinates. The telluric distortion tensor is factorized in three linearly independent 2×2 matrices and a scalar, i.e.

$$C = gTSA$$

where g, the site gain, is a scalar, T, S and A are the twist, shear and anisotropy respectively. The twist (T) and shear (S) tensors represent the determinable portion of the distortion matrix. They affect both the amplitude and the phase of Z_{2D}. Both, the site gain, g, and the anisotropy tensor, A, are the indeterminable parts of the distortion matrix that scale the apparent resistivity curves, and make part of the static shifts for each mode (Jones, 1988). This approach makes it possible to determine the appropriate frequency-independent telluric distortion parameters.

A multi-site, multi-frequency tensor decomposition developed by McNeice and Jones (2001) was performed in this study, which is an extension to Groom and Bailey decomposition (1989). A global minimum is sought to determine the most appropriate strike direction and telluric distortion parameters for a range of frequencies and a set of sites. The application of tensor decomposition analysis suggests a strike of −10° from 604 to 632 sites and N–S from 634 to 845 sites (McNeice and Jones, 2001). Eventually, considering the 90° ambiguity, accepted in magnetotelluric strike analysis, the strike estimation could be 80° and E–W. Then, the option of strike directions −10° and 0° (N–S) which

was very much compatible with the regional geologic structure was chosen.

The distortion parameters were computed for two period bands (10–100 s) and (100–1000 s) and the results for single-site determination are shown in Fig. 3. Larger shear values are observed near the PC, east of the Valle Fértil Lineament and at the Sierras de Córdoba. In general, twist values are smaller than ±25° in the plains, while larger values are observed near the mountains. At the bottom of Fig. 3 the twist and shear normalized RMS misfits are presented, they are smaller for the long periods band indicating that the best fit of data is for the deepest structures.

Phase tensor analysis was applied at every site. The average skew for periods between 10 s and 1000 s for all sites is shown in Fig. 3. Average skews are smaller than ±5° at most sites and a valid 2D regional

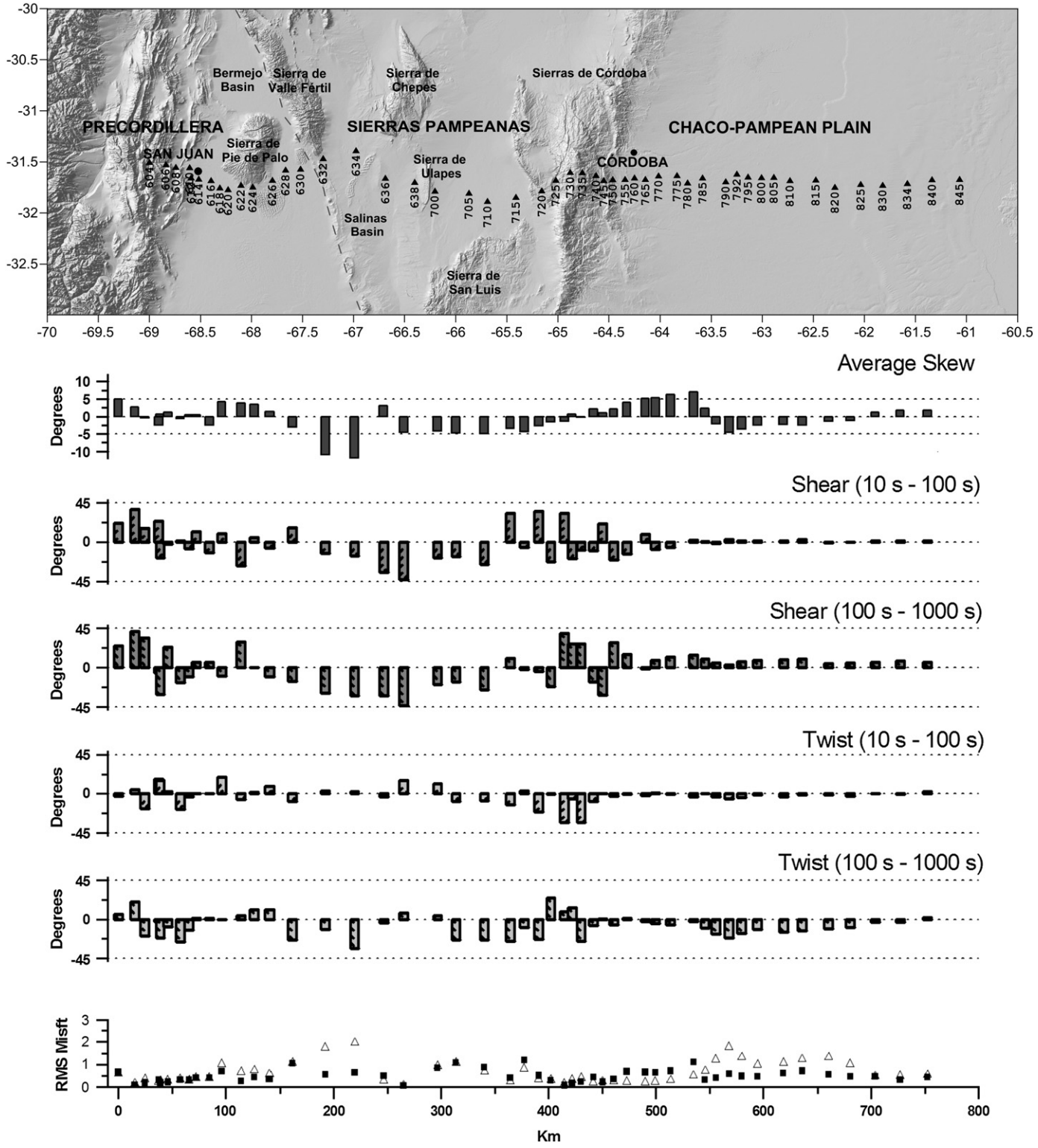

Fig. 3. Average (10–10,000 s) phase tensor skew (2D/3D indicator). Distortion parameters twist and shear, determined at single sites for (10–100 s) and (100–1000 s) bands and their normalized RMS misfits: triangle for (10–100 s) and square for (100–1000 s).

structure interpretation can be assumed, except for sites 634 and 636, where the average skew was around −11° which implies a 3D regional structure. At all the sites, the ellipticity is greater than 0.1. Then, the structure is definitely not 1D.

5.3. Induction vectors

Induction vectors are widely used to analyze bidimensionality. In a two-dimensional situation, they are normal to strike and point towards current concentrations (Parkinson convention). They were analyzed for all sites and periods. The induction vectors real parts for two periods (160 s and 1280 s) are shown in Fig. 4. The magnitude is less than 0.5 except for short periods at the sites close to the Valle Fértil Lineament (sites 624 to 638) where they are much larger and large magnitudes are also observed both for short and long periods in the Chaco-Pampean Plain between sites 775 and 810, pointing significantly to the east.

From site 616 to site 720, induction vectors with significant southward direction can be observed, which indicates the presence of a conductive zone at the south of the profile. In general, the trend of induction vectors is similar for both, short and long periods, except in the Sierras de Córdoba where they are pointing westward for the short periods and eastward for the long ones.

5.4. 2D model

Data inversion was calculated using the non-linear conjugate-gradient (NLCG) algorithm of Rodi and Mackie (2001) in the WingLink MT package. This algorithm minimizes the objective function

$$S = \chi^2 + \tau P(\mathbf{m}).$$

$P(\mathbf{m})$ is a structure penalty function, τ is the trade-off parameter chosen to get the resulting model ($\mathbf{m}$) with the minimum structure (as measured by the structure penalty) for the resulting misfit, χ.

In this study, the penalty is a weighted integral of the Laplacian squared of the model. The weight increases with both, horizontal, α, and vertical derivatives by a factor equal to the vertical scale of each model element, β, and grows with depth and horizontal distance outside the profile; both parameters were set to 1.

Two side-constraints were applied in the inversion over the initial 1000 Ωm half space: i) the effect of the conductive ocean west off the coast of Chile, considered as a layer of 4 km thick with a conductance distribution simulating the actual ocean bathymetry, and ii) a 3 Ωm resistivity was used to simulate the conductive mantle deeper than 650 km as expected by the average global decrease.

The inversion was performed with an error floor large enough to avoid fitting the TE ρ in order to reduce the inherent 3-D distortion in TE mode (highly probable effect present along a 700 km profile) and error floors 10% to TM ρ, 2.9° to both phases and 0.01 absolute value of *Tzy*.

The regularization parameter, τ, was found through several inversions with different values of τ. With decreasing τ, data misfit and smoothness decrease. Large Normalized Root Means Square (NRMS) misfit causes a smoother model at the expense of a worse data fit. The optimum τ, was obtained by the trade-off curve between the smoothness of the model and NRMS misfit. Considering this curve for τ values from 1000 to 0.3, a

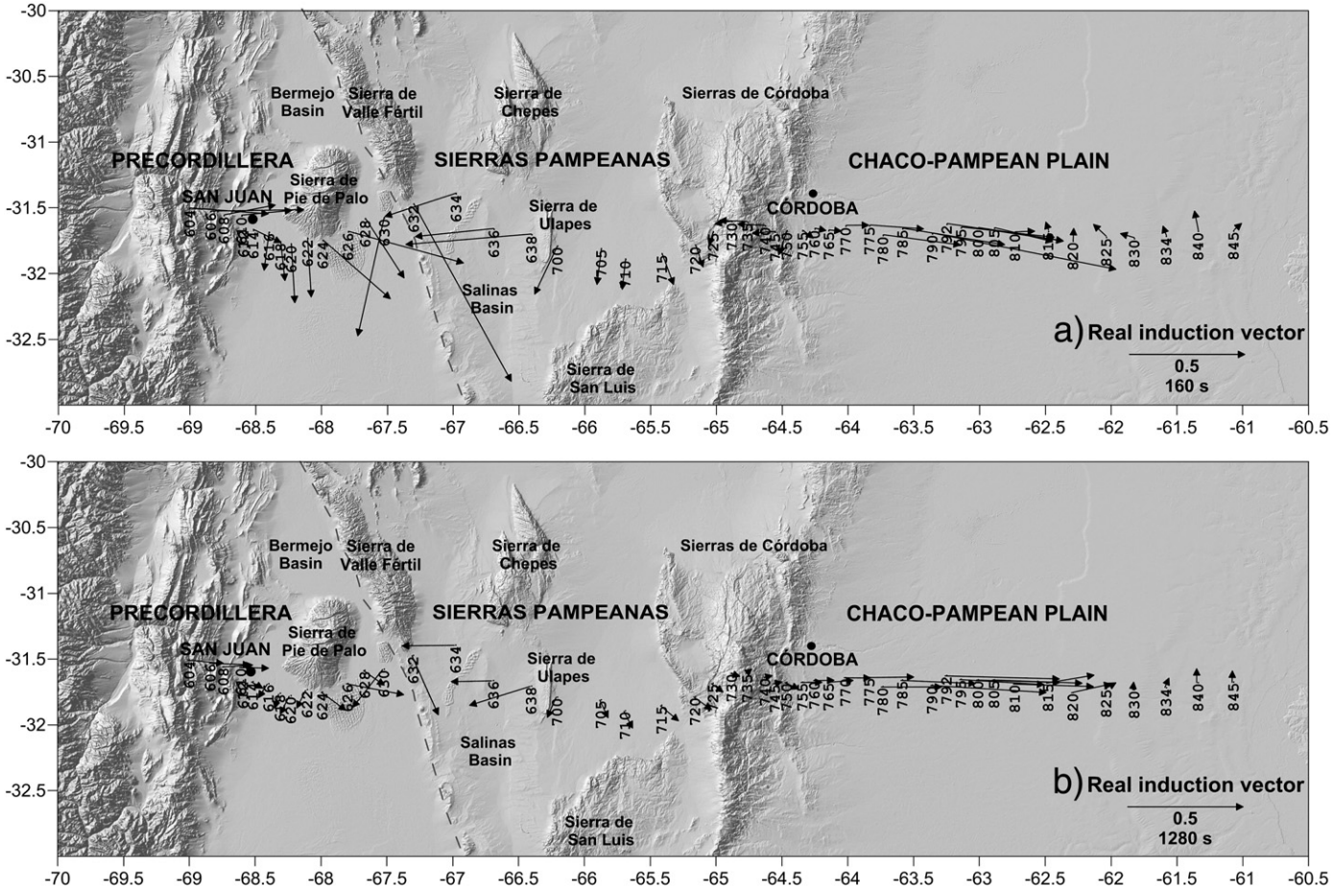

Fig. 4. Induction vectors determined at 160 s and 1280 s for all the sites. In a two dimensional situation, they are normal to strike and point towards current concentration (Parkinson's convention).

value of $\tau = 3$ was used in the final model, shown in Fig. 5. Models obtained for $\tau \leq 1$ showed more detailed structure considered to be an effect of over fitting data. This final inversion was performed with data from all sites with a final NRMS of 1.7 at convergence.

6. Results

A resistivity model along a 700 km profile is shown up to 350 km deep in Fig. 5.This model shows a significant variation in the resistivity structure of the crust and upper mantle.

The shallowest levels with low resistivity (<10 Ωm) found up to 5–8 km deep represent the sedimentary cover along the entire profile and correspond to the Bermejo, Salinas and Chaco-Paranaense basins, from west to east.

The high resistivity levels (>1000 Ωm) found up to 30–15 km depth correspond to the Precordillera (PC) and the Sierras Pampeanas (SP) basement and the resistivity observed below these structures is less than 250 Ωm.

From sites 604 to 740, three conductors (less than 50 Ωm) are observed beneath the PC to the SP. These conductors present differences in thickness and horizontal extension.

From site 745 to the east, a thick resistivity block (>10,000 Ωm) corresponding to the Río de la Plata craton (RPC) appears up to around 140 km deep. A less resistive zone (~200 Ωm) is found in this block, between sites 790 and 834.

7. Interpretation and discussion

To facilitate interpretation, the MT model together with the earthquake hypocenter distribution and the zone where the Moho discontinuity has been determined by different seismological studies is shown in Fig. 6. At the top of this figure, the topographic map with the MT sites and the boundaries between terranes and craton is shown. Fig. 6a shows the geoelectrical model up to 350 km deep and the earthquake hypocenter distribution from CHARGE. These events allowed inferring the depth of the Nazca slab. Fig. 6b shows the geoelectrical model up to 100 km and the different Moho depth determination from Table 1. Fig. 6c shows the "p" axis calculated for focal mechanisms from NEIC catalogue in the study area.

The PC and the Pie de Palo basement are shown as a single high resistivity structure (>1000 Ωm) from the western end of the profile to site 624 approximately. The average thickness is 30 km, being thinner on the eastern edge of the Sierra de Pie de Palo. This basement zone is known as the Cuyania Terrane (Astini et al., 1995; Ramos et al., 1996).

The basement of the SP extends from the Sierra de Valle Fértil (VF) to the eastern edge of the Sierras de Córdoba (SC) with an average thickness of 15 km. This basement is known as Pampia Terrane (Ramos et al., 1996).

The upper–lower crust boundary was identified by strong resistivity contrast between the two layers that suggests the Upper Crustal discontinuity (UCD in Fig. 6a).

From PC to the SP, three deep conductive zones, A, B and C (shown in Fig. 6a) are considered to be within the lower crust. A deep resistive zone (DRZ>1000 Ωm, Fig. 6) which appears up to 120 km deep lies between conductive zones B and C.

Given that distinct changes in resistivity across the Moho are not always present (see e.g. Jones and Ferguson, 2001), MT is not a suitable method to define the crust boundary. However, the bottom of conductors A, B and C could be correlated with the greatest thickness obtained by seismology shown in Fig. 6b.

Earthquake hypocenters make it possible to define the longitude to which interplate coupling is greatest, this indicates that up to that point (around 69.5°W) the mechanical contrast between the two crusts is greater. To the east, the fact that seismicity is not limited to the interface allows to infer that coupling between the two plates is smaller.

That point coincides, at surface, with the eastern edge of the Cordillera Frontal (Valle Uspallata–Calingasta). The resistivity of the lithospheric mantle varies horizontally between 150 Ωm and 250 Ωm.

Wagner et al. (2005) used regional P and S wave travel time data to obtain 3D seismic tomography models for *Vp*, *Vs*, and *Vp*/*Vs* ratios above

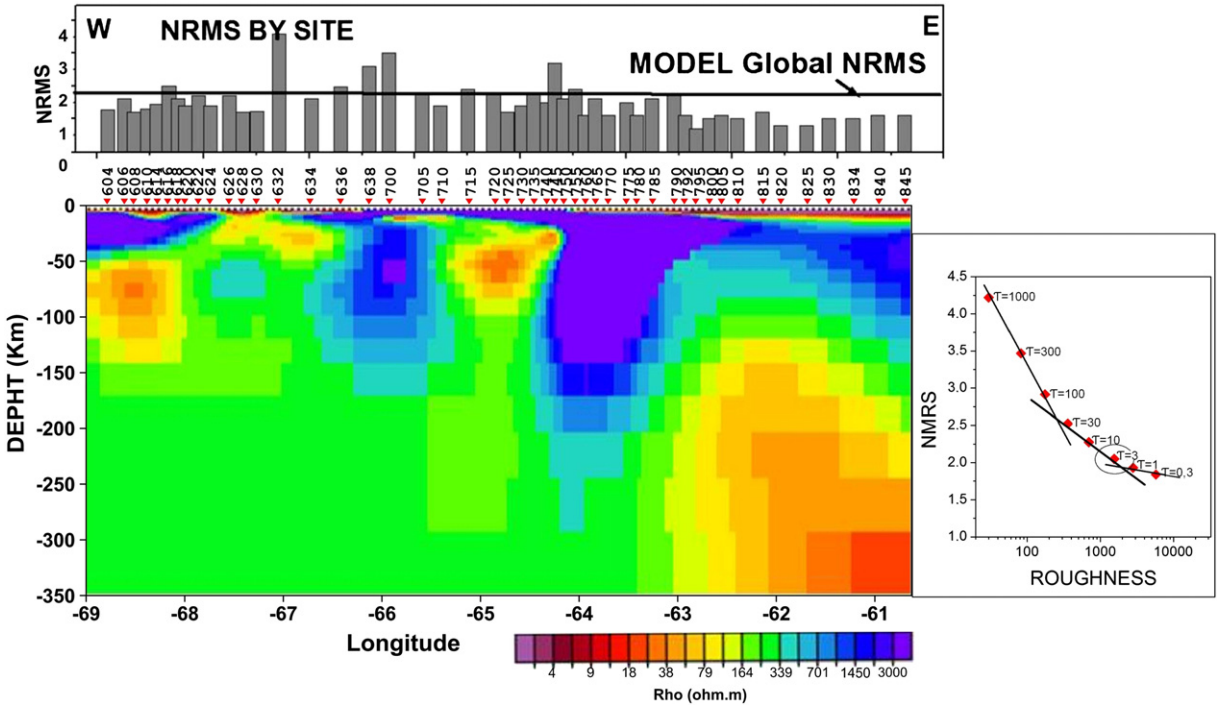

Fig. 5. 2D resistivity model, NRMS by site and trade-off of data misfit with model roughness (Tau = 3 was adopted for the final model).

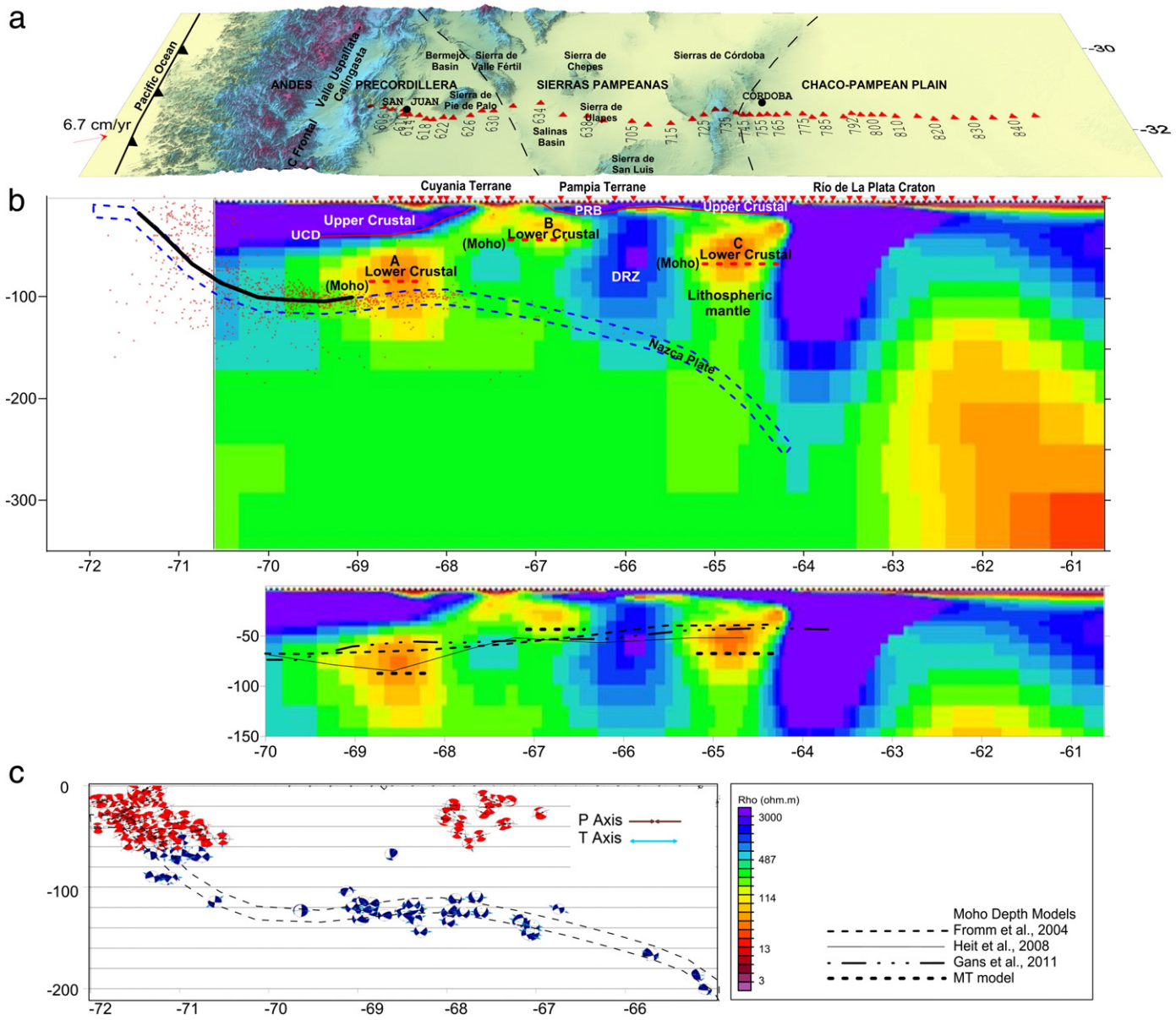

Fig. 6. a) Topographic map and MT sites showing boundaries between terranes and craton. Geoelectrical model up to 350 km deep; Upper Crust Discontinuity (UCD); A, B and C conductors corresponding to the lower crust; DRZ > 1000 Ωm (deep resistive zone) and the earthquake hypocenter distribution from CHARGE catalogue (USGS, 2009). b) Geoelectrical model up to 100 km and the different Moho depth determination from Table 1. c) "p" axis calculated for focal mechanisms (NEIC) in the study area.

the subducting Nazca plate where flattens at 100 km deep. They found low *Vp*, high *Vs*, and low *Vp*/*Vs* ratios, which are unusual results, the tendency of *Vp*/*Vs* ratios to decrease with decreasing temperatures may point to an especially cold lithosphere, the absence of water combined with a lack of present-day heat could explain the lack of volcanism at the surface and the low *Vp*/*Vs* ratios indicate no significant quantities of serpentine above the flat slab. In summary, they suggest a cold, unmelted, unserpentinized lithospheric mantle.

A small number of heat flow observations in the SP and PC are reported. In the central part of this area, only two temperature bottom-hole measurements, connected to oil exploration activity, are available (Robles, 1987). Other measurements have been made from geothermal methods (Uyeda et al., 1978; Hamza and Muñoz, 1996).

Ruiz and Introcaso (2004) showed a map of regional heat flow based on the depth of the Curie point isotherm, which shows that the heat flow pattern in PC is different from that found in SP. The thermal flow lowest values (between 43 and 60 Mw ml^{-2}) are related to Western PC, from which a quick flow increases towards the Valle Fértil Lineament. Meanwhile, higher values (from 55 to 80 Mw ml^{-2}) were found in SP. It is worth pointing out that the maximum flow pattern in NE–SW direction, involving southern PC, Sierra de Pie de Palo, center of Sierra de Valle Fértil and northern Sierra de Los Llanos, could be related to the Juan Fernández Ridge hotspot track.

The highly conductive anomalies, A, B and C, correspond to areas of foreland deformation from the PC to the SP, along 500 km (from sites from 604 to 750), it is located east of the point (69.5°W) where interplate coupling is lower. In this area, different ultramafic belts along shear zones have been identified and associated with ophiolite complex and interpreted as sutures of the terranes accreted to Gondwana margin during the Proterozoic–early Paleozoic. These shear zones were reactivated by Cenozoic faulting (Ramos, 1994; Schmidt et al., 1995), and their roots must necessarily be at the levels of ductile

lower crust (Tikoff et al., 2002). The zone where the lower crust is closer to the surface (B conductive area) coincides with the areas of greatest structural relief and erosion. The interface between the folded ductile lower crust and the brittle upper crust, might act as the main level of décollement of the neighboring structures between the PC, Pie de Palo and the SP. In addition, the geometry of the interface might be conditioning the vergence of those structures.

Seismic hypocenters of deep earthquakes show a subhorizontal slab around 120 km deep, within which bulge-shape geometry causes a slight and unusual westward dip. This tendency was also observed by Alvarado et al. (2009), Anderson et al. (2007), Cahill and Isacks (1992) and Wagner et al. (2005).

The bulge shape in the subducted slab determined by the hypocenters could be produced by: i) a torsion effect generated by the transition from flat to steep subduction along the Andean margin, ii) the effect of the Juan Fernández Ridge subduction (Alvarado et al., 2009), and/or iii) a restriction on the eastward motion by the presence of a deep resistive zone (DRZ, in Fig. 6). Independently of the origin of the bulge shape in the subducted slab, this geometry is possibly related to the steepening of the plate and consequent flow of hot fluids and volatiles from the asthenosphere. Thus, in the context of flat subduction, the onset of steepening would explain the source of heat. The possible presence of upwelling of conductive asthenospheric material may be correlated with long period induction arrows pointing to the east (see Fig. 4b).

The source heat related to the steepening of the subducted slab, was in evidence by a conductive zone rising from the deeper mantle (at least 250 km deep, below the highest elevation of the Sierras de Córdoba), highly indicative of the possible presence of partial melt (Booker et al., 2004).

McKenzie and Jackson (2002) suggest that the lower crust only flows when viscosity is significantly reduced either by heating from igneous intrusions or by the addition of water. Thus, both heating of the lower crust and dehydrating of the uppermost mantle tend to generate a viscosity contrast that favors lower crustal flow. Crustal flow requires that the viscosity of the lower crust be smaller than that of the mantle. Laboratory data suggest that an absolute reduction in viscosity occurs with a small melt fraction (even less than 7%) (Rosenberg and Handy, 2005).

Jordan et al. (1983) and Smalley et al. (1993) suggested that increased interplate coupling above flat slab regions could be responsible for thick skinned deformation in the upper plate, resulting in large scale block uplifts as in the SP. Additionally, we suggest that the development of brittle–ductile transition related to the folding of ductile lower crust might be directly related to the exhumation mechanism of the SP according to Tikoff et al. (2002) concepts.

The MT model shows that the subsurface décollements of the Valle Fértil Lineament correspond to the place where the brittle–ductile transition is tilted eastward and associated with an important source of crustal earthquakes. The "p" axis calculated for focal mechanisms (NEIC) in the area is subparallel to the discontinuity indicating a westward vergence, opposite to the Andean vergence (Fig 6c).

One of the most remarkable features in the MT model is the presence of a large resistive zone (DRZ) which appears below the crystalline basement of the Sierra de Ulapes, having a maximum thickness of 100 km, which decreases westward (57 km). This zone is in contact with the eastern edge of the bulge of the slab. The high resistivity of this area forces the slab to subduct at a higher angle. One hypothesis is that this resistive zone corresponds to a portion of cold and rigid lithosphere, whose upper boundary appears to be separated from the upper crust by a thin conductor possibly related to the lower crust, which might suggest delamination of the crustal roots. This could be an acceptable interpretation from the process point of view: developed eastward migration of magmatic activity during flattening of the slab, thermal weakening of the crust that produces a wave of shortening and consequent crustal thickening which lead to phase transformation from mafic granulite facies to eclogite in the lower crust (Kay et al., 1996; Meissner and Mooney, 1998). The eclogitization of crustal roots and subsequent steepening of the oceanic slab with incoming heat from the asthenosphere leads to delamination.

For the eastern end of the profile and based on both the geological information and the MT results, Favetto et al. (2008) showed an interesting conclusion about the boundary between two crustal units located along the eastern border of the Sierra Chica de Córdoba (site 745), which suggests the transition between the RPC and the Pampia Terrane, that were juxtaposed during the Early–Middle Cambrian Pampean Orogeny (Kraemer et al., 1995). From sites 780 to 845, RPC has a zone of thickness loss due to the presence of anomalous asthenospheric conductive material.

8. Conclusions

This study was performed to detect the geometry of the cortical central Andes in the Andean foreland, from the Precordillera to the Chaco-Pampean Plain close to 31.5°S. The resulting 2D model shows the structure up to 350 km deep. This model was fully discussed taking into account previous geological and geophysical studies. The thickness of the crust is larger in the western than in the eastern side of VFL. There is a good correlation between this feature and the cortical depth inferred by other methods.

In the lower crust, ductile flow was inferred from conductive channels A, B and C. These zones are spatially correlated with the areas of foreland deformation from Precordillera to Sierras Pampeanas. Shear zones reactivated by Cenozoic faulting should have their roots at the levels of the ductile lower crust associated with the conductive channels. Zones where the lower crust is closer to the surface coincide with the areas of greatest structural relief and erosion. The interface between the folded ductile lower crust and the brittle upper crust, might act as the main level of décollement of the neighboring structures between the PC, Pie de Palo and the SP. In addition, the geometry of the interface might be conditioning the vergence of those structures.

The geometry of the subducted slab observed from earthquakes shows a "bulge" shape with an anomalous dip to the west. This smooth slab deformation might be produced by the restriction on the eastward motion due to the presence of an anomalous resistive zone. This particular geometry allows hot fluids and volatiles from the deeper asthenospheric wedge reach the lower crust reducing its viscosity and letting it flow.

Acknowledgments

This research was supported by National Science Foundation grants EAR99-09390 and EAR0310113 and by Agencia Nacional de Promoción Científica y Tecnológica PICT 2005 no. 38253. The MT systems were provided by the EMSOC Instrument Facility supported by NSF grants EAR02-36538 and EAR96-16421. The authors thank Gabriel Giordanengo (INGEIS) for his valuable technical assistance during the surveys.

References

Aceñolaza, F.G., Miller, H., Toselli, A.J., 2002. Proterozoic–Early Paleozoic evolution in western South America — a discussion. Tectonophysics 354, 121–137.

Alvarado, P., Beck, S., Zandt, G., Araujo, M., Triep, E., 2005. Crustal deformation in the southcentral Andes backarc terranes as viewed from regional broadband seismic waveform modeling. Geophysical Journal International 163 (2), 580–598. http://dx.doi.org/10.1111/j.1365246X. 2005.02759.x.

Alvarado, P., Beck, S., Zandt, G., 2007. Crustal structure of the south-central Andes Cordillera and backarc region from regional waveform modelling. Geophysical Journal International 170, 858–875. http://dx.doi.org/10.1111/j.1365-246X.2007.03452.x.

Alvarado, P., Pardo, M., Gilbert, H., Miranda, S., Anderson, M., Saez, M., Beck, S., 2009. Flat slab subduction and crustal models for the seismically active Sierras Pampeanas region of Argentina. Backbone of the Americas: Shallow Subduction, Plateau Uplift, and Ridge and Terrane Collision. Geol. Soc. Am. Memoirs, vol. 204. Geological Society of America, Boulder, CO, pp. 261–278.

Alvarado, P., Sánchez, G., Saez, M., Castro de Machuca, B., 2010. Nuevas evidencias de la actividad sísmica del terreno Cuyania en la región de subducción de placa horizontal de Argentina. Revista Mexicana de Ciencias Geológicas 27, 278–291.

Anderson, M., Alvarado, P., Zandt, G., Beck, S., 2007. Geometry and brittle deformation of the subducting Nazca Plate, Central Chile and Argentina. Geophysical Journal International 171, 419–434. http://dx.doi.org/10.1111/j.1365-246X.2007.03483.x.
Astini, R.A., Benedetto, J.L., Vaccari, N.E., 1995. The early Paleozoic evolution of the Argentine Precordillera as a Laurentian rifted, drifted, and collided terrane: a geodynamic model. Geological Society of America Bulletin 107, 253–273.
Barazangi, M., Isacks, B.L., 1976. Spatial distribution of earthquakes and subduction of the Nazca Plate beneath South America. Geology 4, 686–692.
Basei, M.A.S., Siga Jr., O., Masquelin, H., Harara, O.M., Reis Neto, J.M., Preciozzi, F., 2000. The Dom Feliciano Belt and the Río de la Plata Craton: tectonic evolution and correlation with similar provinces of southwestern Africa. In: Cordani, U.G., Milani, E.J., Thomaz Filho, A., Campos, D.A. (Eds.), Tectonic Evolution of South America, 31st International Geological Congress, Río de Janeiro, Brazil, pp. 311–334.
Bedrosian, P.A., Unsworth, M.J., Egbert, G.D., Thurber, C.H., 2004. Geophysical images of the creeping San Andreas Fault: implications for the role of crustal fluids in the earthquake process. Tectonophysics 385. http://dx.doi.org/10.1016/j.tecto.2004.02.010.
Bevis, M., Isacks, B.L., 1984. Hypocentral trend surface analysis: probing the geometry of Benioff Zones. Journal of Geophysical Research 89, 6153–6170.
Bibby, H.M., Caldwell, T.G., Brown, C., 2005. Determinable and non-determinable parameters of galvanic distortion in magnetotellurics. Geophysical Journal International 163 (3), 915–930.
Booker, J., Favetto, A., Pomposiello, M.C., 2004. Low electrical resistivity associated with plunging of the Nazca flat slab beneath Argentina. Nature 429, 399–403.
Cahill, T., Isacks, B., 1992. Seismicity and shape of the subducted Nazca plate. Journal of Geophysical Research 97 (B12), 17503–17529.
Caldwell, T.G., Bibby, H.M., Brown, C., 2004. The magnetotelluric phase tensor. Geophysical Journal International 158, 457–469.
Calkins, J.A., Zandt, G., Gilbert, H.J., Beck, S.L., 2006. Crustal images from San Juan, Argentina, obtained using high frequency local event receiver functions. Geophysical Research Letters 33 (7), L07309.
Caminos, R., 1979. Sierras Pampeanas de Tucumán, Catamarca, La Rioja y San Juan. In: Turner, J.C.M. (Ed.), Segundo Simposio Geología Regional Argentina. Academia Nacional de Ciencias, Córdoba, pp. 41–80.
Cingolani, C.A., Dalla Salda, L.H., 2000. Buenos Aires cratonic region. In: Cordani, U.G., Milani, E.J., Thomas Filho, A., Campos, D.A. (Eds.), 31st International Geological Congress, Río de Janeiro, pp. 139–146.
Cobbold, P.R., Rossello, E.A., Roperch, P., Arriagada, C., Gómez, L.A., Lima, C., 2007. Distribution, timing, and causes of Andean deformation across South America. In: Ries, A.C., Butler, R.W.H., Graham, R.H. (Eds.), Deformation of the continental crust: the legacy of Mike Coward: Geological Society, London, Special Publications, 272, pp. 321–343.
Dalla Salda, L.H., 1999. Cratón del Río de la Plata, 1: Basamento granítico-metamórfico de Tandilia y Martin Gracia. An. Inst. Geol. Recur. Miner (SEGEMAR), 29, pp. 97–100.
Egbert, G., 1997. Robust multiple station magnetotelluric data processing. Geophysical Journal International 130, 475–496.
Favetto, A., Pomposiello, C., López de Luchi, M., Booker, J., 2008. 2D magnetotelluric interpretation of the crust electrical resistivity across the Pampean terrane — Río de la Plata suture, in central Argentina. Tectonophysics 459, 54–65.
Finney, S.C., 2007. The parauthochtonous Gondwanan origin of the Cuyania (greater Precordillera) terrane of Argentina. A re-evaluation of evidence used for support an allochthonous Laurentian origin. Geologica Acta 5 (2), 127–158.
Fromm, R., Zandt, G., Beck, S.L., 2004. Crustal thickness beneath the Andes and Sierras Pampeanas at 30°S inferred from Pn apparent phase velocities. Geophysical Research Letters 31, L06625. http://dx.doi.org/10.1029/2003GL019231.
Gans, C., Beck, S., Zandt, G., Gilbert, H., Alvarado, P., Anderson, M., Linkimer, L., 2011. Continental and oceanic crustal structure of the Pampean flat slab region, western Argentina, using receiver function analysis: new high-resolution results. Geophysical Journal International 186, 45–58. http://dx.doi.org/10.1111/j.1365-246X.2011.05023.x.
Gilbert, H., Beck, S., Zandt, G., 2006. Lithospheric and upper mantle structure of central Chile and Argentina. Geophysical Journal International 165 (1), 383–398. http://dx.doi.org/10.1111/j.1365246X. 2006.02867.x.
Glover, P., Ádám, A., 2008. Correlation between crustal high conductivity zones and seismic activity and the role of carbon during shear deformation. Journal of Geophysical Research 113, B12210. http://dx.doi.org/10.1029/2008JB005804.
González Bonorino, F., 1950. Algunos problemas geológicos de las Sierras Pampeanas. Asociación Geológica Argentina, Revista 5 (3), 81–110.
Groom, R.W., Bailey, R.C., 1989. Decomposition of magnetotelluric impedance tensors in the presence of local three-dimensional galvanic distortion. Journal of Geophysical Research 94, 1913–1925.
Groom, R.W., Bailey, R.C., 1991. Analytic investigations of the effects of near-surface three-dimensional galvanic scatterers on MT tensor decompositions. Geophysics 56, 496–518.
Gutscher, M.A., Spakman, W., Bijwaard, H., Engdahl, E.R., 2000. Geodynamics of flat subduction: seismicity and tomographic constraints from the Andean margin. Tectonics 19, 814–833. http://dx.doi.org/10.1029/1999TC001152.
Hamza, V.M., Muñoz, M., 1996. Heat flow map of South America. Geothermics 25, 599–646.
Hartmann, L.A., Santos, J.O.S., Cingolani, C.A., McNaughton, N.J., 2003. Two Palaeoproterozoic orogenies in the evolution of the Tandilia Belt, Buenos Aires, as evidenced by zircon U–Pb SHRIMP geochronology. International Geology Review 44, 528–543.
Hasegawa, A., Sacks, I.S., 1981. Subduction of the Nazca Plate beneath Peru as determined from seismic observations. Journal of Geophysical Research 86, 4971–4980.
Heit, B., Yuan, X., Bianchi, M., Sodoudi, F., Kind, R., 2008. Crustal thickness estimation beneath the southern Central Andes at 30 degrees S and 36 degrees S from S wave receiver function analysis. Geophysical Journal International 174 (1), 249–254.
Hyndman, R.D., Shearer, P.M., 1989. Water in the lower continental crust: modelling magnetotelluric and seismic reflection results. Geophysical Journal International 98, 343–365.
Introcaso, A., Lion, A., Ramos, V.A., 1987. La estructura profunda de las Sierras de Córdoba. Revista de la Asociación Geológica Argentina 42 (1–2), 177–187.
Introcaso, A., Pacino, M.C., Fraga, H., 1992. Gravity, isostasy and Andean. Crustal shortening between latitudes 30 and 35 degrees S (in Andean geodynamics). Tectonophysics 205 (1–3), 31–48.
James, D.E., Sacks, S., 1999. Cenozoic formation of the Central Andes: a geophysical perspective. In: Skinner, B. (Ed.), Geology and Mineral Deposits of Central Andes: Society of Economic Geology Special Publication, 7, pp. 1–25.
Jones, A.G., 1988. Static shift of magnetotelluric data and its removal in a sedimentary basin environment. Geophysical 53, 967–978.
Jones, A.G., Ferguson, L.J., 2001. The electric Moho. Nature 409, 331–333.
Jordan, T.E., Allmendinger, R.W., Brewer, J.A., Ramos, V.A., Ando, C.J., 1983. Andean tectonics related to geometry of subducted Nazca plate: Geological Society of America. Bulletin 94, 341–361. http://dx.doi.org/10.1130/00167606.
Kay, S.M., Mpodozis, C., Ramos, V.A., Munizaga, F., 1991. Magma source variations for mid to late Tertiary volcanic rocks erupted over a shallowing subduction zone and through a thickening crust in the Main Andean Cordillera (28–33°S). In: Harmon, R.S., Rapela, C. (Eds.), Andean Magmatism and Its Tectonic Setting: Geological Society of America Special Paper, 265, pp. 113–137.
Kay, S.M., Orrell, S., Abbruzzi, J.M., 1996. Zircon and whole rock Nd–Pb isotopic evidence for a Grenville age and a Laurentian origin for the basement of the Precordillera terrane in Argentina. Journal of Geology 104, 637–648.
Kraemer, P.E., Escayola, M.P., Martino, R.D., 1995. Hipótesis sobre la evolución tectónica neoproterozoica de las Sierras Pampeanas de Córdoba (308400–328400). Revista de la Asociación Geológica Argentina 50, 47–59.
Leech, M.L., 2001. Arrested orogenic development: eclogitization, delamination, and tectonic collapse. Earth and Planetary Science Letters 185, 149–159.
Losito, G., Schnegg, P.A., Lambelet, C., Viti, C., Trova, A., 2001. Microscopic scale conductivity as explanation of magnetotelluric results from the Alps of Western Switzerland. Geophysical Journal International 147, 602–609.
McGlashan, N., Brown, L., Kay, S., 2008. Crustal thickness in the Central Andes from teleseismically recorded depth phase precursors. Geophysical Journal International 175 (3), 1013–1022.
McKenzie, D., Jackson, J., 2002. Conditions for flow in the continental crust. Tectonics 21 (6), 1055. http://dx.doi.org/10.1029/2002TC001394.
McNeice, G.W., Jones, A.G., 2001. Multisite, multifrequency tensor decomposition of magnetotelluric data. Geophysics 66 (1), 158–173.
Meissner, R., Mooney, W.D., 1998. Weakness of the lower continental crust: a condition for delamination, uplift, and escape. Tectonophysics 296, 47–60.
Ortiz, A., Zambrano, J.J., 1981. La provincia geológica Precordillera Oriental. Actas 8° Congreso Geológico Argentino, 3, pp. 59–74.
Pankhurst, R.J., Rapela, C.W., 1998. The proto-Andean margin of Gondwana: an introduction. In: Pankhurst, R.J., Rapela, C.W. (Eds.), The proto-Andean margin of Gondwana: Geological Society, London, Special Publication, 142, pp. 1–9.
Pankhurst, R.J., Ramos, A., Linares, E., 2003. Antiquity and evolution of the Río de la Plata craton in Tandilia, southern Buenos Aires province, Argentina. Journal of South American Earth Sciences 16, 5–13.
Parkinson, W.D., 1962. The influence of continent and oceans in geomagnetic variations. Geophysical Journal of the Royal Astronomical Society 6, 441–449.
Ramos, V.A., 1994. Terranes of southern Gondwanaland and their control in the Andean structure (30–33°S lat.). In: Reutter, K.J., Scheuber, E., Wigger, P.J. (Eds.), Tectonics of the Southern Central Andes, Structure and Evolution of an Active Continental Margin. Springer, Berlin, pp. 249–261.
Ramos, V., Vujovich, G.I., Kay, S.M., McDonough, M., 1993. Las Orogénesis de Grenville en las Sierras Pampeanas Occidentales: La Sierra de Pie de Palo y su Integración al Supercontinente Proterozoico. XII Congreso Geológico Argentino y II Congreso de Exploración de Hidrocarburos, 3, pp. 343–357.
Ramos, V.A., Cegarra, M., Cristallini, E., 1996. Cenozoic tectonics of the High Andes of west-central Argentina, (30°–36°S latitude). Tectonophysics 259, 185–200.
Ramos, V., Cristallini, E.O., Pérez, D.J., 2002. The Pampean flat slab of the Central Andes. Journal of South American Earth Sciences 15, 59–78.
Rapela, C.W., Pankhurst, R.J., Casquet, C., Baldo, E., Saavedra, J., Galindo, C., Fanning, C.M., 1998. The Pampean Orogeny of the southern proto-Andes: Cambrian continental collision in the Sierras de Córdoba. In: Pankhurst, R.J., Rapela, C.W. (Eds.), The proto-Andean margin of Gondwana: Geological Society of London, Special Publication, vol. 142, pp. 181–217.
Rapela, C.W., Casquet, C., Baldo, E., Dahlquist, J., Pankhurst, R.J., Galindo, C., Saavedra, J., 2001. Lower Paleozoic Orogenies at the proto-Andean margin of South America, Sierras Pampeanas, Argentina. Journal of Iberian Geology 27, 23–41.
Rapela, C.W., Fanning, M., Pankhurst, R.J., 2005. The Rio de la Plata craton: the search for its full extent. In: Pankhurst, R.J., Veiga, G. (Eds.), Gondwana 12, Mendoza 2005. Abs Academia Nacional de Ciencias, p. 304.
Regnier, M., Chiu, J.M., Smalley Jr., R., Isacks, B.L., Araujo, M., 1994. Crustal thickness variation in the Andean foreland, Argentina, from converted waves. Bulletin of the Seismological Society of America 84 (4), 1097–1111.
Robles, D., 1987. El gradiente geotérmico actual en Argentina y zonas aledañas de países vecinos. 10° Cong. Geol. Argentino, Actas, 2, pp. 313–316.
Rodi, W., Mackie, R., 2001. Nonlinear conjugate gradient algorithm for 2-D magnetotelluric inversion. Geophysics 66, 174–178.
Rosenberg, C., Handy, M.R., 2005. Experimental deformation of partially melted granite revisited: implications for the continental crust. Journal of Metamorphic Geology 23, 19–28.
Rossello, E.A., Limarino, C.O., Ortiz, A., Hernández, N., 2005. Cuencas de los Bolsones de San Juan y La Rioja. In: Chebli, G.A., Spalletti, L.A., Cortiñas, J.S., Legarreta, L., Vallejo, E.L. (Eds.), Frontera Exploratoria de la Argentina. Instituto Argentino del Petróleo, Buenos Aires, pp. 147–173. Cap. 7.

Ruiz, F., Introcaso, A., 2004. Curie point depths beneath Precordillera Cuyana and Sierras Pampeanas obtained from spectral analysis of magnetic anomalies. Gondwana Research 7 (4), 1133–1142.
Saalmann, K., Hartmann, L.A., Remus, M.V.D., Koester, E., Conceição, R.V., 2005. Sm–Nd isotope geochemistry of metamorphic volcano-sedimentary successions in the São Gabriel Block, southernmost Brazil: evidence for the existence of juvenile Neoproterozoic oceanic crust to the east of the Rio de la Plata craton. Precambrian Research 136, 159–175.
Schmidt, C.J., Astini, R.A., Costa, C.H., Gardini, C.E., Kraemer, P.E., 1995. Cretaceous rifting, alluvial fan sedimentation and Neogene inversion, southern Sierras Pampeanas, Argentina. In: Tankard, A.J., Suárez Soruco, R., Welsink, H.J. (Eds.), Petroleum basins of South America: American Association of Petroleum Geologists, Memoir AAPG, Tulsa, Oklahoma 62, pp. 341–358.
Shalivahan, Bhattacharya, B.B., 2002. Implications of novel results about Moho from magnetotelluric Studies. Current Science 83 (10).
Shankland, T., Ander, M., 1983. Electrical conductivity, temperatures, and fluids in the lower crust. Journal of Geophysical Research 88, B11. http://dx.doi.org/10.1029/JB088iB11p09475, 1983.
Smalley, R. Jr, Pujol, J., Regnier, M., Chiu, J.M., Chatelain, J.L., Isacks, B.L., Araujo, M., Puebla, N., 1993. Basement seismicity beneath the Andean Precordillera thin-skinned thrust belt and implications for crustal and lithospheric behaviour. Tectonics 12, 63–76. http://dx.doi.org/10.1029/92TC01108.
Soyer, W., Unsworth, M.J., 2006. Deep electrical structure of the northern Cascadia subduction zone (British Columbia, Canada): implications for the role of fluids. Geology 34, 53–56. http://dx.doi.org/10.1130/G21951.1, 2006.
Thomas, W.A., Astini, R.A., 2003. Ordovician accretion of the Argentine Precordillera terrane to Gondwana: a review. Journal of South American Earth Sciences 16, 67–79. http://dx.doi.org/10.1016/S0895-9811(03)00019-1.
Tikoff, B., Teyssier, Ch, Waters, Ch, 2002. Clutch tectonics and the partial attachment of lithospheric layers. European Geosciences Union, Stephan Mueller Special Publication Series, 1, pp. 57–73.
Unsworth, M.J., Jones, A.G., Wei, W., Marquis, G., Gokarn, S.G., Spratt, J.E., INDEPTH-MT team, 2005. Crustal rheology of the Himalaya and Southern Tibet inferred from magnetotelluric data. Nature 438. http://dx.doi.org/10.1038/nature04154 (3 2005).
Uyeda, S., Watanabe, T., Volponi, F., 1978. Report of heat flow measurements in San Juan and Mendoza, Argentina. Earthquake Research Institute Bulletin v. 53, 165–172.
USGS, 2009. http://earthquake.usgs.gov/regional/neic/.
Varela, R., Roverano, D., Sato, A.M., 2000. Granito El Peñon, sierra de Umango: descripción, edad Rb/Sr e implicancias geotectónicas. Revista de la Asociación Geológica Argentina 55 (4), 407–413.
Vigny, C., Rudloff, A., Ruegg, J.C., Madariaga, R., Campos, J., Alvarez, M., 2009. Upper plate deformation measured by GPS in the Coquimbo gap, Chile. Physics of the Earth and Planetary Interiors 175, 86–95.
Wagner, L.S., Beck, S., Zandt, G., 2005. Upper mantle structure in the south central Chilean subduction zone (30° to 36°S). Journal of Geophysical Research 110. http://dx.doi.org/10.1029/2004JB003238.
Zapata, T.R., Allmendinger, R.W., 1996. Growth stratal records of instantaneous and progressive limb rotation in the Precordillera thrust belt and Bermejo basin, Argentina. Tectonics 15 (5), 1065–1083.